Available online at www.sciencedirect.com

SciVerse ScienceDirect

Ceramics International 39 (2013) 3759–3764

CERAMICS INTERNATIONAL

www.elsevier.com/locate/ceramint

# Effects of different chelating agents on the composition, morphology and electrochemical properties of $LiV_3O_8$ crystallites synthesized via sol–gel method

Dunqiang Wang, Liyun Cao*, Jianfeng Huang, Jianpeng Wu

*Shaanxi University of Science and Technology, Key Laboratory of Auxiliary Chemistry & Technology for Light Chemical Industry, Xi'an, Shaanxi 710021, China*

Received 28 May 2012; received in revised form 16 October 2012; accepted 17 October 2012
Available online 24 October 2012

**Abstract**

Lithium trivanadate ($LiV_3O_8$) crystallites have been synthesized via sol–gel processing using oxalic, tartaric, citric and malic acid as the chelating agents. The thermal decomposition process of the as-prepared $LiV_3O_8$ precursor was investigated by thermogravimetric (TG) and differential scanning calorimetry (DSC). The structure, morphology and electrochemical performance of the as-synthesized $LiV_3O_8$ samples were characterized by X-ray diffraction (XRD), scanning electron microscopy (SEM) and the galvanostatic charge–discharge test. Different chelating agents were introduced to investigate their effects on the products composition, morphology and electrochemical properties. Result show that the samples prepared with oxalic and tartaric acid are similar to show thin rod-like morphology in submicron size distribution while the samples prepared with citric and malic acid are found consisting of block-like crystallities in micron size. Further electrochemical results exhibit that the $LiV_3O_8$ particles with oxalic, tartaric, citric and malic acid exhibit an initial discharge capacity of 304.4 mA h/g, 296.8 mA h/g, 268.7 mA h/g and 275.3 mA h/g, respectively. After 20 cycles, they retain discharge capacity of 250.2 mA h/g, 237.6 mA h/g, 198.5 mA h/g and 206.8 mA h/g, respectively.


*Keywords:* $LiV_3O_8$; Sol–gel method; Electrochemical properties; Lithium ion batteries

## 1. Introduction

As a promising cathode material for rechargeable lithium batteries, Lithium vanadium oxide ($LiV_3O_8$) has been extensively studied over the past two decades for its attractive electrochemical properties such as high specific energy, good rate capacity, long cycle life, low cost and facile preparation.

The conventional method to synthesize $LiV_3O_8$ is a solid-state reaction at high temperature about 680 °C. The solid-state routes generally are obsessed by the drawbacks such as inhomogeneity, lack of stoichiometry control, and larger particle size. To avoid these drawbacks, great efforts and extensive synthesis routes such as hydrothermal reaction [1,2], microwave assisted solid-state synthesis [3], sol–gel method [4–7], microwave assisted sol–gel method [8], combustion method [9], spray drying synthesis [10], freeze drying technique [11] and spray pyrolysis process [12] have been developed to synthesize and improve the structure, morphology and electrochemical properties of the $LiV_3O_8$ material. Among these routes, sol–gel process is the most commonly used method due to its unique advantages in the synthesis of oxide materials. For instance, the raw materials can be mixed at the molecular level and thus the products possess homogeneous composition and higher capacity. Many works have been done to fabricate $LiV_3O_8$ crystallites by using sol–gel methods in which citric acid was mostly used as chelating agent. However, few works on the effect of other different chelating agents on the product structure, morphology and electrochemical properties were reported.

In the present work, we utilized a low temperature sol–gel process to synthesize the $LiV_3O_8$ cathode material using oxalic

*Corresponding author. Tel.: +86 29 8616 8802; fax: +86 29 861 688 02.
*E-mail addresses:* wongdq1986@163.com (D. Wang), lycao505@163.com (L. Cao).

0272-8842/$ - see front matter © 2012 Elsevier Ltd and Techna Group S.r.l. All rights reserved.
http://dx.doi.org/10.1016/j.ceramint.2012.10.214

acid, citric acid, tartaric acid and malic acid as chelating agents, respectively. The influences of different chelating agents on the phase composition, morphology and electrochemical properties of the products were particularly investigated.

## 2. Experimental

### 2.1. Sample preparation

The chemical reagents used in the experiments are lithium hydroxide ($LiOH \cdot H_2O$), ammonium metavanadate ($NH_4VO_3$), oxalic acid ($H_2C_2O_4$), tartaric acid ($C_4H_6O_6$), citric acid ($C_6H_8O_7 \cdot H_2O$) and malic acid ($C_4H_6O_5$), all of which are of analytical grade and used without any purification.

The typical synthesis process is briefly described as follows. Firstly, stoichiometric amounts of $LiOH \cdot H_2O$ and $NH_4VO_3$ (Li:V=1:3, molar ratio) were mixed in deionized water (100 mL). For each experiment, the solution of oxalic acid, tartaric acid, citric acid and malic acid was added to the mixture under constant magnetic stirring, respectively. The ratio of total amount of metal ions to each chelating agent was 1:2. The mixture was heated to 80 °C with stirring for 1 h, and then a clear blue color solution was obtained. Next, the solution was placed at 80 °C for 12 h to form a gel. The gel was washed with absolute ethyl alcohol twice to remove the remaining water with a later drying in a vacuum oven at 120 °C for 5 h to obtain the precursor. Finally the precursor was ground and then calcined at 350 °C and 500 °C for 4 h to produce the powders, respectively. After cooling to room temperature naturally in the furnace, the powders were reground to obtain the final $LiV_3O_8$ products.

### 2.2. Characterization

The thermal decomposition process of the precursor was analyzed by thermogravimetric (TG) and differential scanning calorimeters (DSC) using a NETZSCH STA 409PC thermal analyzer at the heating rate of 15 °C/min in air from room temperature to 700 °C. The crystal structures of the as-prepared powders were investigated by X-ray diffractometry (XRD) using a Rigaku D/max-2000 powder diffractometer with a graphite monochromatic Cu$K\alpha$ radiation ($\lambda$=0.15418 nm) in the $2\theta$ range of 5–70°. The particle morphology, particle size and particle size distribution of the samples were observed with a JEOL JSM-6460 scanning electron microscopy (SEM).

### 2.3. Electrochemical measurements

The cathode was fabricated by compressing a mixture of 80 wt% active materials (the as-synthesized $LiV_3O_8$ samples), 10 wt% carbon black and 10 wt% polyvinylidene fluoride (PVDF) on to a pure Al foil and then drying in vacuum at 120 °C for 24 h. The cells were assembled in an argon-filled glove box with the concentrations of moisture and oxygen below 2 ppm, lithium foil as anode and Celgard 2320 film as separator. The electrolyte was 1 M $LiPF_6$ in ethylene carbonate (EC) and dimethyl carbonate (DMC) in volume ratio of 1:1. The capacity and cycling performance of the electrode were performed on a galvanostatic charge–discharge method using Land battery measurement system (CT2001A, WuHan, PR China) at a current density of 50 mA/g in the potential range of 2.0–4.0 V (vs. $Li^+/Li$). All tests were performed at room temperature.

## 3. Results and discussion

### 3.1. Thermal analysis

Fig. 1 shows the TG-DSC curves of the $LiV_3O_8$ precursor obtained by sol–gel method using different chelating agents. Clearly, step-like curves of weight loss for all the four gel precursors are obtained. The TG-DSC curves of precursor prepared by tartaric acid (Fig. 1b), citric acid (Fig. 1c) and malic acid (Fig. 1d) are very similar. There were three main steps of thermal decomposition observed on the TG-DSC curves of the precursors (Fig.1b–d). In the first step ranged from room temperature to about 250 °C, there is an endothermic peak due to the vaporization of water and ammonia. The corresponding weight loss is about 10 wt% in this process. At the second step ranged from 250 °C to 450 °C, strong exothermic peaks are observable due to the vigorous combustion reactions of the residual organics. In this stage, a large amount of $CO_2$ and $H_2O$ is released because of the combustion of carboxylic acid. And the weight loss of this process is about 43 wt%, 30 wt%, 54 wt% for the three TG curves, respectively. The last step is from 450 °C to 700 °C, an exothermic peak and an endothermic peak are found in this stage. The former one at about 570 °C is due to continuous decomposition of the precursor and the completion of the crystallization reaction. The latter one at about 680 °C is ascribed to the melting of the $LiV_3O_8$. For all the three curves, there is no obvious weight loss after about 620 °C, and the weight loss of this process is about 18 wt%, 14 wt% and 20 wt%, respectively. For the precursor prepared by oxalic acid (Fig. 1a), two distinct steps of weight loss were observed on the TG-DSC curve. The initial weight loss occurred in range of room temperature to 250 °C is mainly assigned to the vaporization of water and ammonia which correspond to the endothermic peak at 152 °C. The weight loss is about 16 wt% in this process. The second stage is from 250 °C to 370 °C and the weight loss is about 48 wt%. A rapid weight loss at this step indicates the precursor burned acutely and oxalic salts broke down into $CO_2$ and $H_2O$ to volatilize. The exothermic peak at 370 °C can be attributed to the complete decomposition of the organic groups and crystallization of $LiV_3O_8$. There is no major weight loss after 370 °C, up to a temperature of 700 °C on the TG curve. But there is an endothermic peak observed at 616 °C and this is attributed

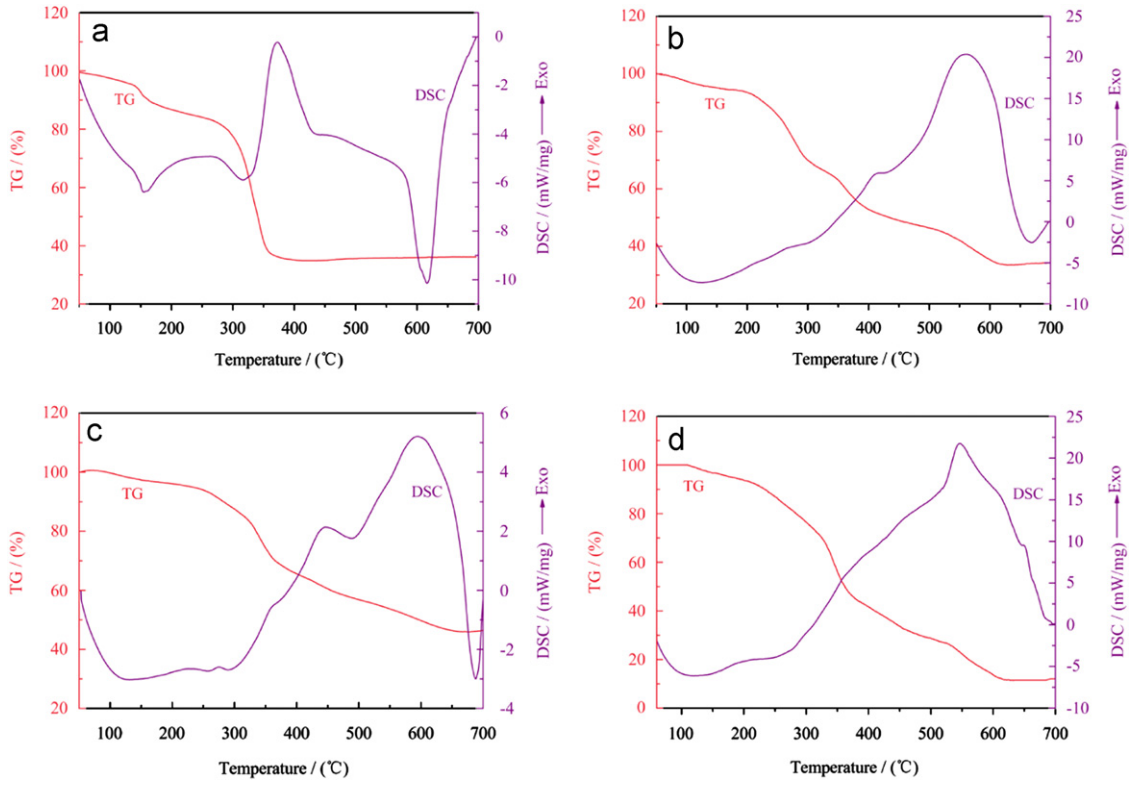


Fig. 1. TG-DSC curves of The $LiV_3O_8$ precursors prepared by using different chelating agents: (a) oxalic acid; (b) tartaric acid; (c) citric acid and (d) malic acid.

to the melting of $LiV_3O_8$. This means that the precursor prepared by oxalic acid can be decomposed completely at relative lower temperature compared with other three precursors, making the nucleation process completed at the early stage of the sol–gel process.

### 3.2. XRD analysis

The XRD patterns of the samples prepared with different chelating agents at 350 °C are shown in Fig. 2. The XRD patterns are consistent well with the known layered-type $LiV_3O_8$ (JCPDS No. 72-1193), meaning that these $LiV_3O_8$ samples have a monoclinic crystalline structure and belong to the $P2_1/m$ space group. But the pattern of the sample prepared with citric acid (curve *c*) shows a small impurity peak at $2\theta$ of 12.3°, which can be attributed to phase of $Li_{0.3}V_2O_5$ (JCPDS No. 18-0755). This $Li_{0.3}V_2O_5$ impurity phase has also been observed in the synthesis of $LiV_3O_8$ by other methods [13–16]. There are two possible reasons for the presence of $Li_{0.3}V_2O_5$ impurity. On the one hand, the ratio of Li/V at some local areas in the precursor is not 1:3, because the decomposition of the organic groups is not finished yet under this condition, which leads $Li^+$ ions to diffuse insufficiently into the $V_3O_8$ layers. On the other hand, part of the LiOH may be volatilized or part of the $LiV_3O_8$ may be decomposed. It shows that the four patterns are mostly similar to each other. The main difference is the relative intensity of some peaks of $LiV_3O_8$.

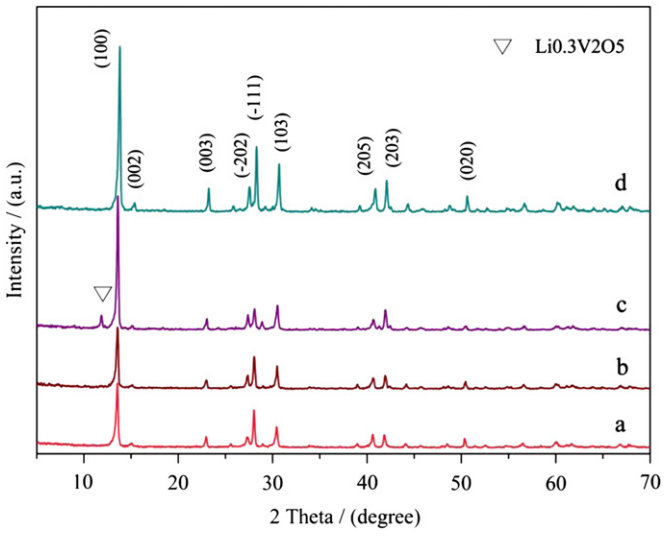


Fig. 2. XRD patterns of $LiV_3O_8$ powders obtained by using different chelating agents at 350 °C: (a) oxalic acid; (b) tartaric acid; (c) citric acid and (d) malic acid.

The intensity of (1 0 0) and (0 0 2) peaks of sample c and d are much higher than those of sample a and b, which indicates that the bigger grain size and higher crystallinity of $LiV_3O_8$ are formed. Given different intensity of the (1 0 0) peak results in different level of orientation along the (1 0 0) plane. For $LiV_3O_8$ with layer structure, the

higher intensity of (1 0 0) peak will cause stronger (1 0 0) plane preferred orientation and relatively long diffusion paths for lithium ions, which is disadvantageous to reversible insertion/extraction of Lithium ions between the $V_3O_8^-$ layers [17].

Apparently, not all lithium can diffuse and distribute uniformly into the $V_3O_8^-$ layers, due to diverse chelating agents and the different chemical state of the metal ions in the precursor. Therefore, $LiV_3O_8$ crystallites with different crystallinity, grain size and crystallization orientation can be obtained by choosing different chelating agents.

According to the TG-DSC analysis, the organics in the precursors would nearly decompose completely after 500 °C. Therefore, the XRD patterns of the powders obtained at 500 °C were also investigated. Fig. 3 shows that all patterns are similar and no impurity phases are detected, indicating the achievement of pure $LiV_3O_8$ of all samples. As the calcinations temperature increased to 500 °C, the diffraction peaks of all samples became sharper and higher than those of samples obtained at 350 °C, which indicates the increase in crystallinity and grain size of the powders. It also can be seen that the four patterns have a little shift compared with each other. In the calcinations process, $NH_3$, $CO_2$ and $H_2O$ will be produced due to the decomposition of the organics. These inorganic molecules may be intercalated and deintercalated during the synthesis of $V_3O_8^-$ puckered layers. And this may cause the shift of the XRD peaks.

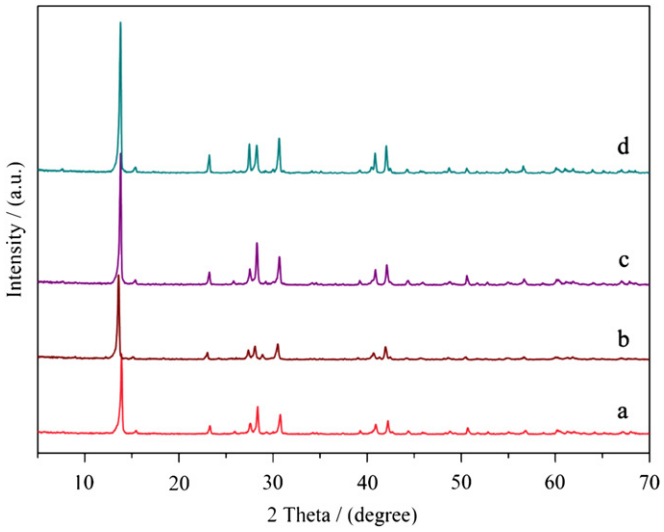


Fig. 3. XRD patterns of $LiV_3O_8$ powders obtained by using different chelating agents at 500 °C: (a) oxalic acid; (b) tartaric acid; (c) citric acid and (d) malic acid.

Generally, the brown color of the material after calcinations process is typical of $LiV_3O_8$ [13,18]. In this study, the color of the products obtained at the same calcination temperature by different chelating agents is not the same as each other. For the samples obtained at 350 °C, the color of sample a and b are brown before and after grinding in a mortar, while those of sample c and d are blue black before grinding. But after grinding in a mortar by hand, the color is changed to brown. For the samples obtained at 500 °C, the color of sample a is still brown before and after grinding. The colors of other three samples are a little blue black before grinding, and it is changed to dark brown after grinding. The phenomenon is similar to a recent report by Pan et al. [18]. The blue black color before grinding may be attributed to the residual carbon from the decomposition of chelating agent, which is in agreement with the TG-DSC analysis above (Fig. 1). The $CO_2$ generated by the decomposition of the sol may intercalate into the $V_3O_8^-$ layers and the residual carbon may cover the surface of the $LiV_3O_8$ particles, and therefore the blue black color presents before grinding.

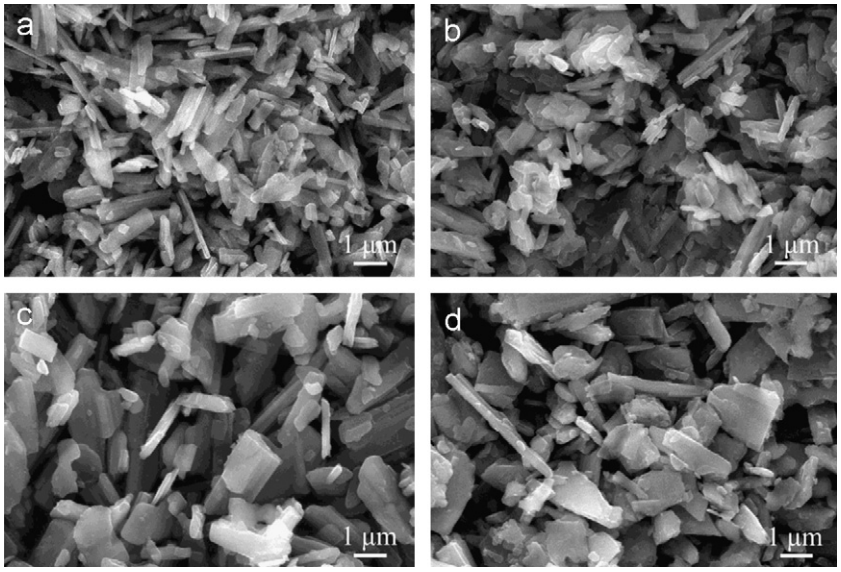


Fig. 4. SEM images of the $LiV_3O_8$ powders prepared with different chelating agents at 350 °C: (a) oxalic acid; (b) tartaric acid; (c) citric acid and (d) malic acid.

### 3.3. SEM analysis

Fig. 4 shows the SEM images of the $LiV_3O_8$ powders synthesized with different chelating agents at 350 °C. The morphologies of the $LiV_3O_8$ powders synthesized by oxalic acid (Fig. 4a) and tartaric acid (Fig. 4b) are similar. Both of them show thin rod-like crystallites morphology with thickness of 50–200 nm, 100–500 nm in width and 0.5–2 μm in length. The morphologies of the $LiV_3O_8$ powders synthesized by citric acid (Fig. 4c) and malic acid (Fig. 4d) show a block-like structure in micrometer scale. Some small particles appear among the crystallites and the particle size distribution is less homogeneous than that of the former two samples. The intercalation process of lithium ions between the layers of the cathode is a diffusion process. Therefore the $LiV_3O_8$ crystallites with smaller particles and lower crystallinity have higher activated specific surface area, which may shorten the diffusion paths for the lithium ions inserted between $(V_3O_8)^-$ layers, which can lead to higher specific capacity and better cycle stability.

In the sol–gel process, the chelating agents have a significant influence on obtaining excellent phase purity and good stoichiometric inorganic oxides, thus affecting the structure and morphology of the products. The carboxylic acid groups in the chelating agents can form chemical bonds with V ions and Li ions simultaneously to form a homogeneous precursor gel, which offers molecular level mixing of the raw materials with good stoichiometry control. Moreover, the chelating agent acts as an organic fuel during the sintering process decomposed the metal complexes at low temperature. The heat generated in the gel combustion process makes the nucleation process complete at the early stage of the sol–gel process, leading to a narrow size distribution of the $LiV_3O_8$ powders. Smaller particle and well size distribution of $LiV_3O_8$ powders can be obtained by using oxalic and tartaric acid as chelating agents in this work.

### 3.4. Electrochemical properties

The initial discharge curves of the as-synthesized four samples at 350 °C are shown in Fig. 5. It is apparent that there are several discharge patent plateaus during the first charge–discharge cycle, which corresponds to the phase transition between the couples of $Li_{1+x}V_3O_8$ ($x$=0.1–4) on the course of lithium ions insertion/extraction [19,20]. This is the characteristic of the electrochemical process of $LiV_3O_8$. It can be seen that voltage drops heavily from 4.00 V to 2.82 V vs. $Li/Li^+$, which may be attributed to the polarization process resulted from unstable diffusion. At the process of discharge in which $Li^+$ is inserted into the cathode, the voltage drops differently, demonstrating that phase transitions might take place. It shows that the samples prepared by oxalic acid (a), tartaric acid (b), citric acid (c) and malic acid (d) deliver an initial discharge capacity of 304.4 mA h/g, 296.8 mA h/g, 268.7 mA h/g and 275.3 mA h/g at a current density of 50 mA/g, respectively. Among them, the sample prepared by oxalic acid has the highest initial discharge capacity, and this may be attributed to its lower crystallinity and smaller size of the particle, which can make the efficient contact of the material with the electrolyte and provide more active sites for $Li^+$ ions diffusion and accommodation.

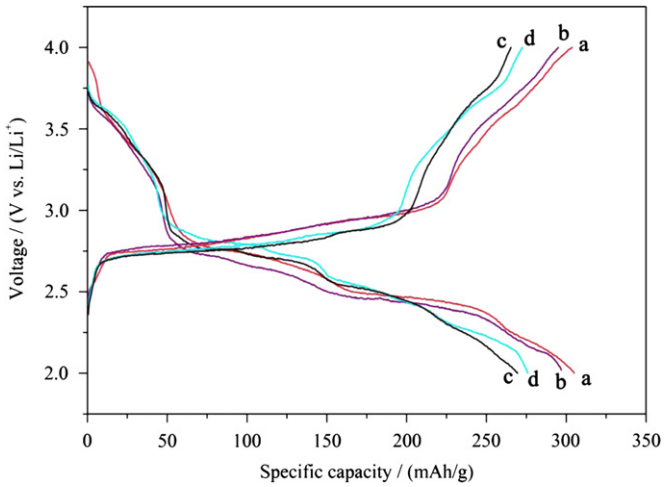


Fig. 5. The initial charge–discharge curves of the samples prepared at 350 °C by: (a) oxalic acid; (b) tartaric acid; (c) citric acid and (d) malic acid.

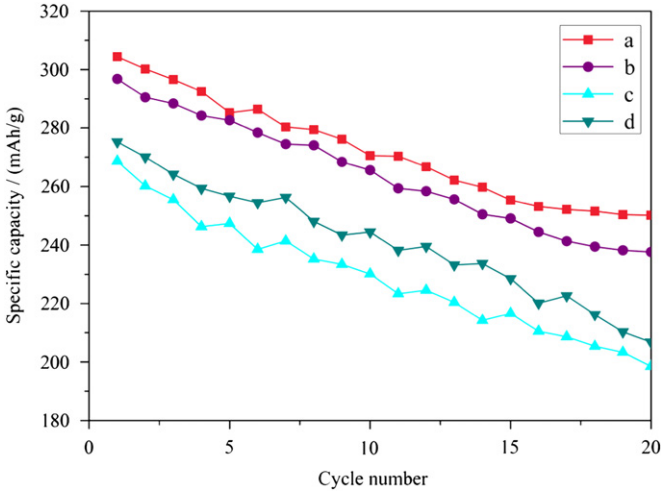


Fig. 6. The cycling performance of the samples prepared at 350 °C by: (a) oxalic acid; (b) tartaric acid; (c) citric acid and (d) malic acid.

Cycling performance of the samples synthesized at 350 °C by oxalic acid (a), tartaric acid (b), citric acid (c) and malic acid (d) is shown in Fig. 6. Important differences in cycle process can be observed in these samples. It can be seen that sample a and b give good cycle performance. The first specific discharge capacity of sample a is 304.4 mA h/g and remains 250.2 mA h/g after 20 cycles. Sample b delivers an initial discharge capacity of 296.8 mA h/g and sustains 237.6 mA h/g after 20 cycles, which is a little lower compared with sample a. In contrast, the specific capacities

of sample c and d remain 198.5 mA h/g and 206.8 mA h/g corresponding to 73.8% and 75.1% of their initial values, respectively. The worse cycling performance of the last two samples may be attributed to many causes, such as the crystallite orientations along (1 0 0) plane, higher crystallinity, larger particle size with wide distribution and longer lithium diffusion paths in the $V_3O_8^-$ layers. Capacity decay of $LiV_3O_8$ probably results from the incomplete reversibility of phase transformation between the $LiV_3O_8$ and $Li_4V_3O_8$ [21], which means that lithium ions cannot be completely inserted into and extracted out of $LiV_3O_8$ during the charge and discharge process.

## 4. Conclusions

$LiV_3O_8$ powders with different particle size and size distribution were successfully synthesized via a sol–gel process using oxalic, tartaric, citric and malic acid as the chelating agents. Results indicated that different chelating agents had strong effects on the particle size, morphology, degree of agglomeration and electrochemical performance of the products. In our study, the products synthesized by oxalic acid and tartaric acid were found to have thin rod-like crystallites morphology in submicron size with homogeneous distribution, exhibiting good electrochemical performances.

## Acknowledgements

This work was supported by the National Natural Science Foundation of China (50942047), Natural Science Foundation of Shaanxi Province of China (2010JM6001), International Science and Technology Cooperation Project of Shaanxi Province (2011kw-11), and the graduate Innovation Foundation of Shaanxi University of Science and Technology.

## References

[1] H.Y. Xu, H. Wang, Z.Q. Song, Y.W. Wang, H. Yan, M. Yoshimura, Novel chemical method for synthesis of $LiV_3O_8$ nanorods as cathode materials for lithium ion batteries, Electrochimica Acta 49 (2004) 349–353.

[2] J.Q. Xu, H.L. Zhang, T. Zhang, Q.Y. Pan, Y.H. Gui, Influence of heat-treatment temperature on crystal structure, morphology and electrochemical properties of $LiV_3O_8$ prepared by hydrothermal reaction, Journal of Alloys and Compounds 467 (2009) 327–331.

[3] G. Yang, G. Wang, W.H. Hou, Microwave solid-state synthesis of $LiV_3O_8$ as cathode material for lithium batteries, The Journal of Physical Chemistry B 109 (2005) 11186–11196.

[4] L. Liu, L.F. Jiao, Y.H. Zhang, J.L. Sun, L. Yang, Y.L. Miao, H.T. Yuan, Y.M. Wang, Synthesis of $LiV_3O_8$ by an improved citric acid assisted sol–gel method at low temperature, Materials Chemistry and Physics 111 (2008) 565–569.

[5] H. Heli, H. Yadegaric, A. Jabbari, Low-temperature synthesis of $LiV_3O_8$ nanosheets as an anode material with high power density for aqueous lithium-ion batteries, Materials Chemistry and Physics 126 (2011) 476–479.

[6] H. Ma, Z.Q. Yuan, F.Y. Cheng, J. Liang, Z.L. Tao, J. Chen, Synthesis and electrochemical properties of porous $LiV_3O_8$ as cathode materials for lithium-ion batteries, Journal of Alloys and Compounds 509 (2011) 6030–6035.

[7] H.L. Zhang, J.R. Neilson, D.E. Morse, Vapor-diffusion-controlled sol–gel synthesis of flaky lithium vanadium oxide and its electrochemical behavior, The Journal of Physical Chemistry C 144 (2010) 19550–19555.

[8] F. Wu, L. Wang, C. Wu, Y. Bai, Structural characterization and electrochemical performance of lithium trivanadate synthesized by microwave sol–gel method, Electrochimica Acta 54 (2009) 4613–4619.

[9] Y.C. Si, L.F. Jiao, H.T. Yuan, et al., Structural and electrochemical properties of $LiV_3O_8$ prepared by combustion synthesis, Journal of Alloys and Compounds 486 (2009) 400–405.

[10] N. Tran, K.G. Bramnik, H. Hibst, J. Prölß, N. Mronga, M. Holzapfel, W. Scheifele, P. Novák, Spray-drying synthesis and electrochemical performance of lithium vanadates as positive electrode materials for lithium batteries, Journal of The Electrochemical Society 155 (2008) A384–A389.

[11] O.A. Brylev, O.A. Shlyakhtin, A.V. Egorov, Y.D. Tretyakov, Phase formation and electrochemical properties of cryochemically processed $Li_{1+x}V_3O_8$ materials, Journal of Power Sources 164 (2007) 868–873.

[12] S.H. Ju, Y.C. Kang, Morphological and electrochemical properties of $LiV_3O_8$ cathode powders prepared by spray pyrolysis, Electrochimica Acta 55 (2010) 6088–6092.

[13] A.Q. Pan, J. Liu, J.G. Zhang, G.Z. Cao, W. Xu, Z.M. Nie, D. Choi, B.W. Arey, C.M. Wang, S.Q. Liang, Template free synthesis of $LiV_3O_8$ nanorods as a cathode material for high-rate secondary lithium batteries, Journal of Materials Chemistry 21 (2011) 1153–1161.

[14] C. Cheng, Z.H. Li, X.Y. Zhan, Q.Z. Xiao, G.T. Lei, X.D. Zhou, A macaroni-like $Li_{1.2}V_3O_8$ nanomaterial with high capacity for aqueous rechargeable lithium batteries, Electrochimica Acta 55 (2010) 4627–4631.

[15] A. Deptuła, M. Dubarry, A. Noret, J. Gaubicher, T. Olczak, W. Lada, D. Guyomard, A typical $Li_{1.1}V_3O_8$ prepared by a novel synthesis route, electrochem, Solid-State Letters 9 (2006) A16–A18.

[16] Y.M. Liu, X.C. Zhou, Y.L. Guo, Effects of fluorine doping on the electrochemical properties of $LiV_3O_8$ cathode material, Electrochimica Acta 54 (2009) 3184–3190.

[17] F. Wu, L. Wang, C. Wu, Y. Bai, F. Wang, Study on $Li_{1+x}V_3O_8$ synthesized by microwave sol–gel route, Materials Chemistry and Physics 115 (2009) 707–711.

[18] A.Q. Pan, J.G. Zhang, G.Z. Cao, S.Q. Liang, C.M. Wang, Z.M. Nie, B.W. Arey, W. Xu, D.W. Liu, J. Xiao, G.S. Li, J. Liu, Nanosheet-structured $LiV_3O_8$ with high capacity and excellent stability for high energy lithium batteries, Journal of Materials Chemistry 21 (2011) 10077–10084.

[19] S. Jouanneau, A. Le Gal La Salle, A. Verbaere, M. Deschamps, S. Lascaud, D. Guyomard, Influence of the morphology on the Li insertion properties of $Li_{1.1}V_3O_8$, J. Mater. Chem. 13 (3003) 921–926.

[20] S. Jouanneau, A. Le Gal La Salle, A. Verbaere, D. Guyomard, The origin of capacity fading upon lithium cycling in $Li_{1.1}V_3O_8$, Journal of The Electrochemical Society 152 (2005) A1660–A1667.

[21] J. Kawakita, T. Miura, T. Kishi, Charging characteristics of $Li_{1+x}V_3O_8$, Solid State Ionics 118 (1999) 141–147.